12th INTERNATIONAL SCIENTIFIC CONFERENCE ON DEFENSIVE TECHNOLOGIES
OTEH 2026
Serbia, Tara, 21 - 24 October 2026

INFLUENCE OF PROCESS PARAMETERS ON QUALITY OF LASER POWDER BED FUSION PRODUCED AL10SIMG PARTS

ALEKSANDAR ĆITIĆ
Military Technical Institute, Belgrade, aleksandar.citic@mod.gov.rs

VESNA LUKIĆ
Military Technical Institute, Belgrade

JOVANA MANDIĆ
Military Technical Institute, Belgrade

MARKO BOJIN
Military Technical Institute, Belgrade

ALEKSA GRUBIĆ
Military Technical Institute, Belgrade

MILOŠ STEPANOVIĆ
Military Technical Institute, Belgrade

ŽIVORAD JEVTIĆ
Military Technical Institute, Belgrade

Abstract: *This study examines the influence of Laser Powder Bed Fusion (LPBF) process parameters on the quality of AlSi10Mg alloy parts. Two sets of samples were fabricated using different combinations of laser power, scan speed, and hatch spacing, resulting in distinct energy densities. Visual examination revealed that lower energy density resulted in rough surfaces and delamination, indicating insufficient interlayer bonding. Chemical analysis confirmed that all samples met EN AC-Al10SiMg compositional requirements, while hardness measurements showed no significant variation between parameter sets or build orientations. Microstructural observations identified typical LPBF features, including fine cellular Al–Si eutectic and coarse dendritic like grains, with pores more frequent in low-energy samples. The results demonstrate that LPBF process parameters strongly affect surface morphology while having negligible impact on bulk hardness. Optimizing energy density is essential for achieving improved microstructural uniformity and overall part quality in AlSi10Mg components.*

Keywords: *LPBF, Al10SiMg, Process parameters*

1. INTRODUCTION

Additive Manufacturing (AM) enables the production of complex geometries directly from a digital model, without the need for traditional tools or molds. Among various AM techniques, Laser Powder Bed Fusion (LPBF) is most adopted method for manufacturing metal components. The LPBF process uses a high energy laser beam to selectively melt a layer of metal powder, forming parts layer by layer [1, 2] under extremely high cooling rates on the order of $10^6 – 10^8\ °C/s$. Such thermal conditions lead to the formation of a unique microstructure, characteristic of LPBF process, which differs significantly from the microstructures of alloys produced by conventional processes such as casting, rolling or forging [3]. Wide range of metal powders for use in LPBF process is developed such as 316L steel, maraging steel, titanium, nickel, aluminum alloys and others. Al alloys offer good compromise between strength and density, in addition to being inexpensive. Most common Al alloy used in LPBF is Al10SiMg, a hypoeutectic aluminum alloy containing approximately 10% Si with an addition of Mg. This alloy is recognized as highly suitable for AM due to its excellent processability, low density, good corrosion resistance, and favorable mechanical properties. Compared with other metal powders, aluminum alloys still present challenge in the LPBF process due to high reflectivity, high thermal conductivity and low melt viscosity [1, 2, 4]. In the LPBF process, AlSi10Mg forms a fine cellular Al–Si eutectic, with a silicon network distributed around primary aluminum cells, resulting in increased strength and hardness compared to cast alloy states. However, this microstructure simultaneously leads to reduced ductility and increased sensitivity to residual stresses [4]. Components produced from AlSi10Mg are widely used in automotive engineering, aerospace structures, robotics, energy systems, and lightweight mechanical assemblies, where the combination of low weight and high strength is essential [5]. Despite these advantages, the final quality of

Corresponding author: A. Ćitić;
E-mail: aleksandar.citic@mod.gov.rs
DOI: 10.5937/OTEH26131C

LPBF-fabricated AlSi10Mg parts is sensitive to process parameters, which govern melt pool behavior, microstructural evolution, defect formation, and mechanical properties. Key LPBF parameters include laser power, scan speed, hatch spacing, layer thickness, preheating temperature, and scanning strategy. Together, these parameters determine the volumetric energy density delivered to the powder bed, influencing melt pool stability, track geometry, layer bonding, and porosity formation. Insufficient energy input typically leads to lack-of-fusion, while excessive energy can cause keyhole porosity, evaporation of alloying elements, and microstructural inhomogeneity [6]. Hatch spacing affects the overlap between adjacent melt tracks, while scanning strategy influences residual stress distribution and grain texture. Therefore, optimizing process parameters is essential for achieving high density, uniform microstructure, and reliable mechanical properties. In addition to process parameters, the quality of AlSi10Mg powder plays a crucial role. Powder used for LPBF must exhibit spherical morphology, narrow particle size distribution, low oxide content, and good flowability, as deviations can lead to segregation, non-uniform layer deposition, and increased porosity [7]. Recycled powder, although economically attractive, often shows increased oxygen content and altered particle size distribution, which may degrade the mechanical properties of printed parts [8]. Considering all the above, LPBF process parameters have a decisive influence on the quality of AlSi10Mg parts, including their density, microstructure, mechanical properties, defect formation, and long-term reliability. Understanding the interdependence of these parameters is fundamental for process optimization and improving the characteristics of final components.

2. EXPERIMENTAL PROCEDURE

2.1 Material and LPBF process

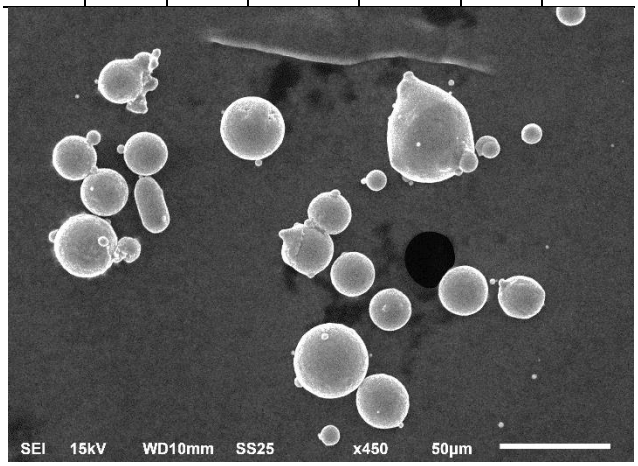
To produce additively manufactured samples, Eplus 3D EP-M450 machine was used. Two sets of samples made of Al10SiMg powder were produced with a different set of process parameters, (Table 1). The laser energy density (E) related to the LPBF process is calculated according to formula [1]:

$$E = \frac{P}{V \cdot H \cdot L_T} \qquad (1)$$

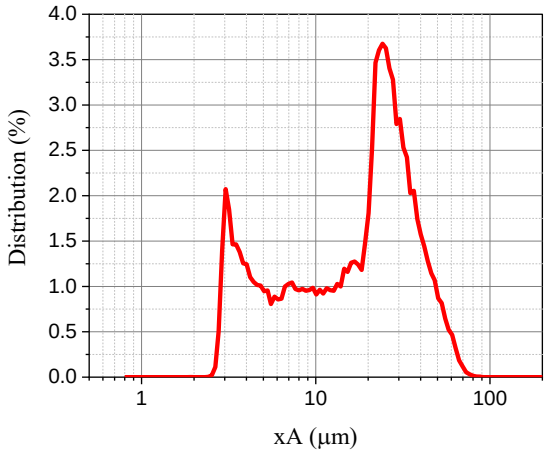
where P is laser power, V is the laser scan speed, H represents hatch distance and L_T is layer thickness. For both sets of sample's, layer thickness was held constant, while other parameters were changed, which gave energy density of 39.3 J/mm^3 for set I, and 50.3 J/mm^3 for set II parameters. For set I, nine identical cubes with dimensions (10x10x10) mm were produced (marked 1-9), and for set II, five identical cubes with dimensions (15x15x10) mm were produced (marked A-E). The morphology and particle size distribution of used powder is shown in Figure 1. Most of the observed powder particles are spherical, and the rest shows ellipsoidal or uneven shape. Particle size ranges from 3 µm to 70 µm, with mean size of 20.2 µm. 10 % of particles have size to 3,6 µm, 50 % of particles have size up to 20,3 µm while 90 % of particles are up to 38,9 µm. Mean value of particle circularity is 0,97. A JEOL JSM-6610LV scanning electron microscope was used to observe the morphology of used powder, while size and circularity were determined on Anton Paar Litesizer DIA 500 instrument

Table 1. Used process parameters

	Laser power P, W	Scan speed V, mm/s	Layer thickness L_T, µm	Hatch distance H, µm	Laser spot size, µm	Energy density E, J/mm^3
Set I	385	1400	50	140	85	39.3
Set II	425	1300	50	130	71	50.3



a) SEM image of powder particles



b) particle size distribution

Figure 1. Morphology and powder particle size distribution.

2.2 Characterization

Visual examination of the manufactured parts was performed after the samples were removed from the build plate, by naked eye and by Leica stereo microscope equipped with DFC 245 camera.

To determine if change in process parameters affected elements evaporation from the powder during melting, chemical composition of the produced samples was analyzed by Optical Energy Spectrometer (OES) Belec Compact Port.

Hardnes was determined by Brinell method (HB 2.5/62.5), according to SRPS EN ISO 6506 standard. Measurements were performed on XY plane (plane parallel to the build plate), and on XZ/YZ plane (plane parallel to the build direction).

For microstructure analysis samples were wet grounded on SiC paper, polished using diamond suspension and etched using Keller A reagent (1 ml HF, 1.5 ml HCL, 2.5 ml HNO_3 and 95 ml H_2O) for 8 s. Samples were observed in polished and etched state on Leitz Metaloplane optical microscope in bright field. Microstructure was analyzed in XY and XZ/YZ plane.

3. RESULTS

3.1. Visual examination

The surface morphology of produced samples is shown on Figure 2 for set I parameters and on Figure 3 for set II parameters. The surface of the samples produced using the parameter set I was visibly rougher than the surface of samples made with parameter set II. Observation under stereo microscope showed that the surface of parameter set I specimens was less uniform, with presence of coarse spherical particles (marked with red arrows) and fine powder particles (marked with yellow arrows), Figure 2a. Additionally, delamination of layers was observed on samples 7, 8, and 9, figure 2b-d.

Samples produced with Set II parameters showed smoother and more uniform surfaces. Although fine powder particles (marked with yellow arrows) were still present, Figure 3, no delamination was observed.

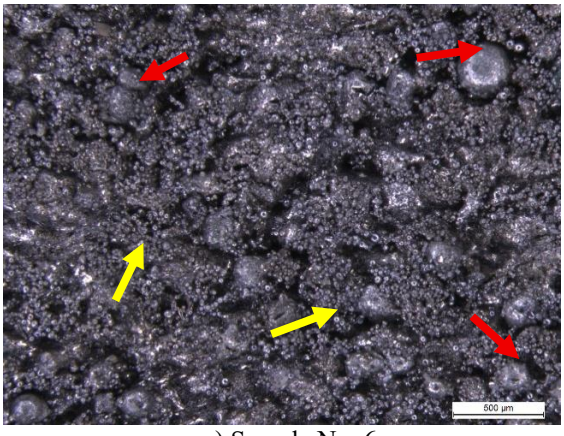
3.2 Chemical composition

The chemical composition of produced samples is given in Table 2.

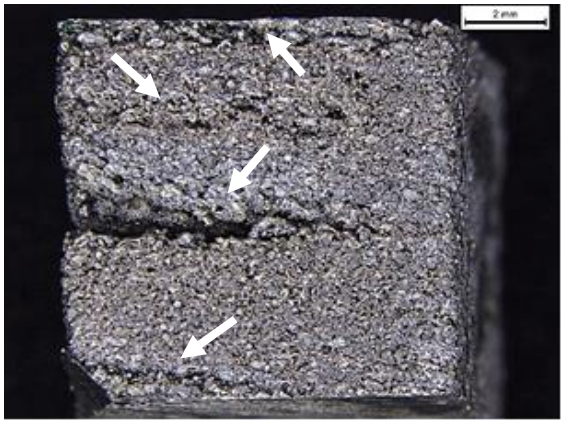
Table 2. Chemical composition of produced samples, mass. %

Element	Set I parameter samples	Set II parameter samples	EN AC-Al10SiMg according to SRPS EN 1706
Si	10.40	10.81	9.0-11.0
Fe	0.21	0.24	max. 0.55
Cu	<0.001	0.002	max. 0.05
Mn	0.008	0.007	max. 0.45
Mg	0.33	0.34	0.20-0.45
Ni	0.03	0.03	max. 0.05
Zn	<0,001	0.01	max. 0.10
Al	Balance	Balance	Balance

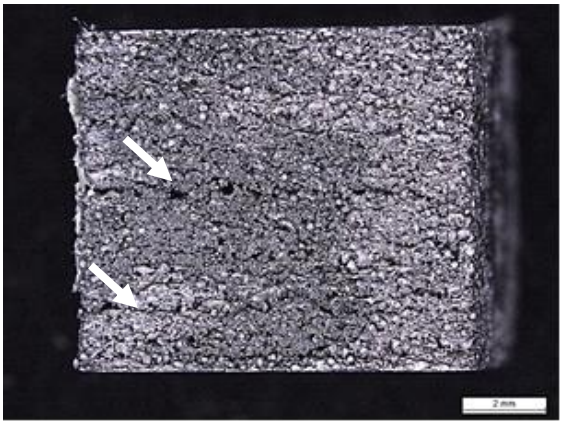
Chemical composition of samples from both sets of parameters is in accordance with standard SRPS EN 1706 for aluminum alloy EN AC Al10SiMg. No significant difference in chemical composition between samples from both sets of parameters is observed.



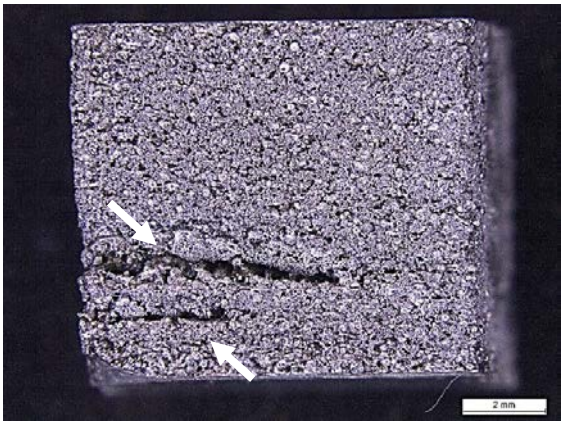
a) Sample No. 6



b) Sample No. 7

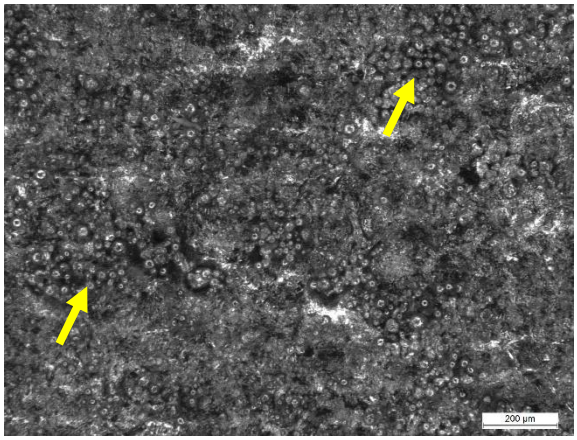


c) Sample No. 8

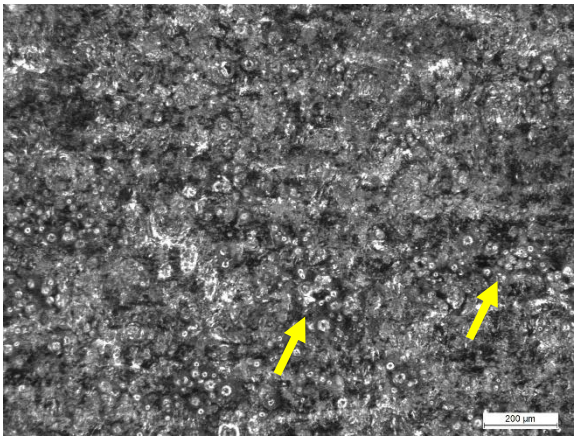


d) Sample No. 9

Figure 2. Surface of the samples produced with Set I parameters.



a) Sample A



b) Sample C

Figure 3. Surface of the samples produced with Set II parameters.

3.3 Hardness measurements

Results of hardness measurements are shown in table 3.

Table 3. Obtained hardness values, HB

	Measurement plane	Hardness, HB	Mean value
Set I	XY	129; 131; 129; 129; 131	130
	XZ/YZ	128; 128; 126; 128, 125	127
Set II	XY	130; 129; 130; 129; 133	130
	XZ/YZ	119; 119; 120; 119	119

3.4 Microstructure

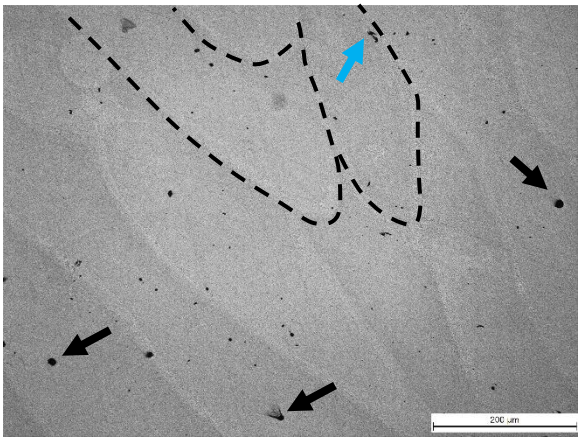
Figure 4 shows typical microstructure of specimens produced using set I parameters in as polished and etched state. Metallurgical defects such as gas pores (marked with black arrows) and lack of fusion (marked with blue arrows) were observed. Apart from the defects, clear melt pool boundaries were also observed in as polished state as well as after etching. On Figure 5 is shown microstructure of samples produced with set II parameters. Microstructure of set II samples also contained metallurgical defects such as pores and lack of fusion. Sporadically, coarse pores were observed. Size of coarse pores is approximately 100 µm in diameter. Comparing set I and set II samples, pores are more frequent in set I samples. Under higher magnification, difference in microstructure between center and edge of melt pool
At the edges microstructure is coarser, while moving away from edges, microstructure changes and becomes

finer (Figure 4b and d, Figure 5b and d) On XY plane microstructure is cell like, while on XZ/YZ plane microstructure is dendrite like (Figure 4f and h, Figure 5f and h).

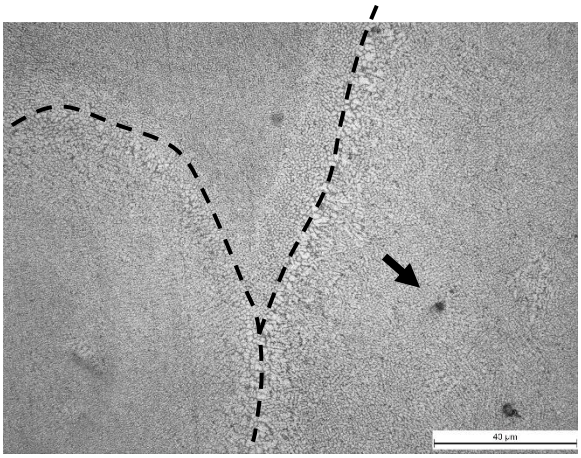
4. DISCUSSION

Visual examination revealed clear differences in surface quality between samples produced with parameter Set I and Set II. Samples produced using Set I parameters exhibited rougher surface, with presence of coarse spherical particles as well as fine powder particles. Additionally, delamination of layers was observed on samples produced using set I parameters suggesting inadequate interlayer bonding and lack-of-fusion defects. Formation of coarse spherical particles and delamination of layers can be attributed to balling effect. High reflectivity and thermal conductivity of Al can lead to formation of molten droplets on the powder bed surface. After solidification, these droplets form spherical particles which are known as balling phenomena [9]. The balling effect leads to uneven scan tracks and weak bonding between layers leading to porosity and delamination. Lack of balling defects and delamination of layers in set II parameter samples is attributed to higher energy density which provides enough molten material to reduce the occurrence of balling effect [9].

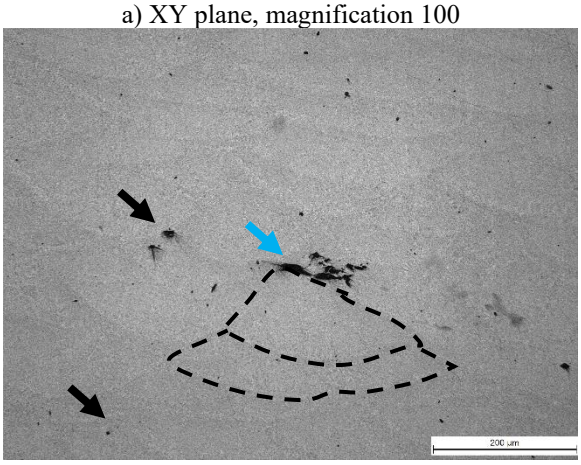
During LPBF process, high energy laser selectively melts metal powder which solidifies instantly as laser moves. This rapid solidification creates unique microstructure characterized by Al matrix and cellular network of Al-Si eutecticum. During solidification, high cooling rates lead to supersaturation of melt pool with silicon. As a result, microstructure exhibits fine Al-Si eutecticum. On Figure 4 and 5, two types of microstructures were observed: coarse and fine cell like and dendrite like. Coarse dendrite like structure grains, during cooling, nucleate and grow at the interface between previously solidified layer and melted phase of new layer. Subsequently, dendrites grow in the direction of heat flux [5, 10].



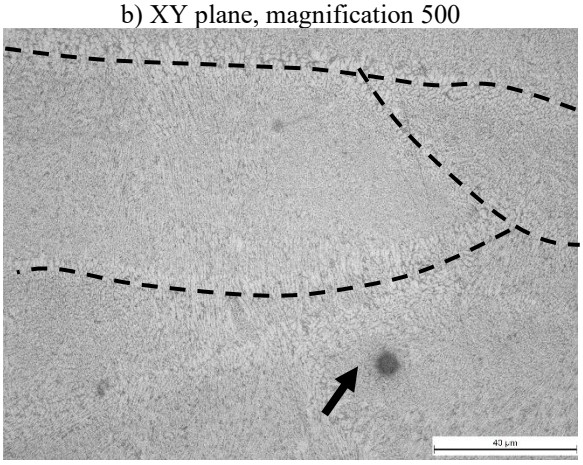
a) XY plane, magnification 100



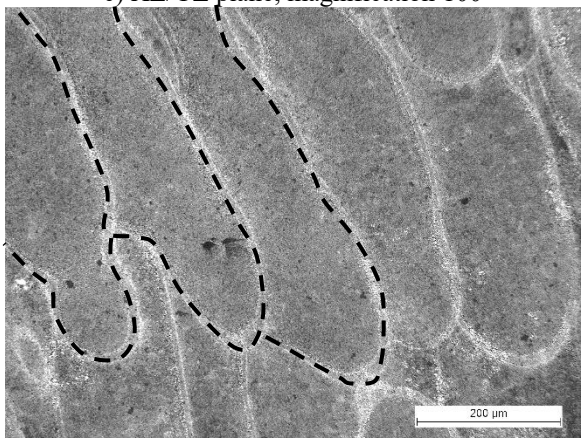
b) XY plane, magnification 500



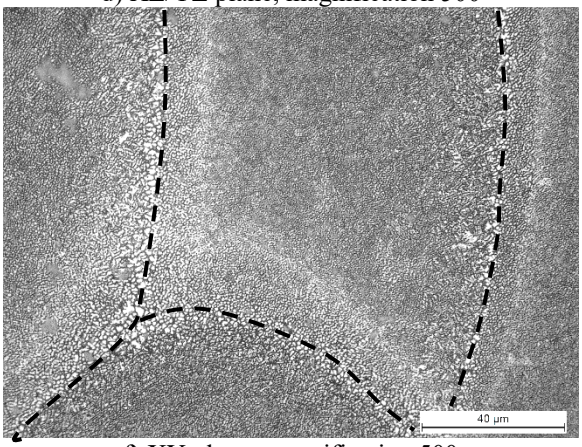
c) XZ/YZ plane, magnification 100



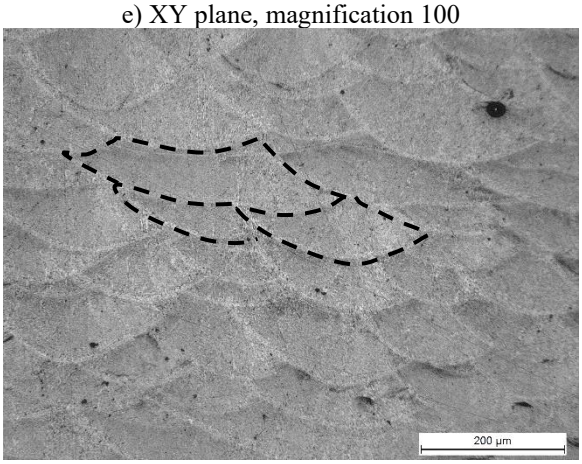
d) XZ/YZ plane, magnification 500



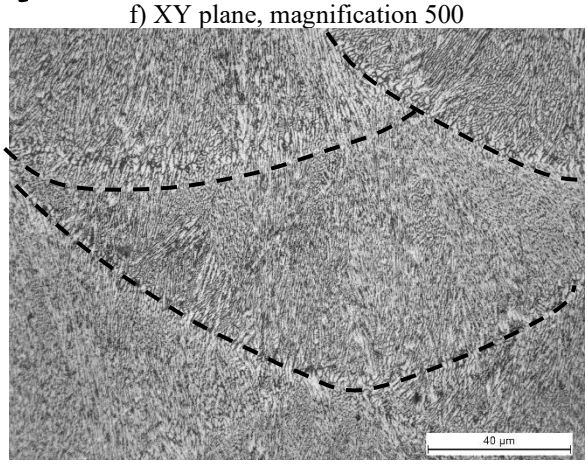
e) XY plane, magnification 100



f) XY plane, magnification 500

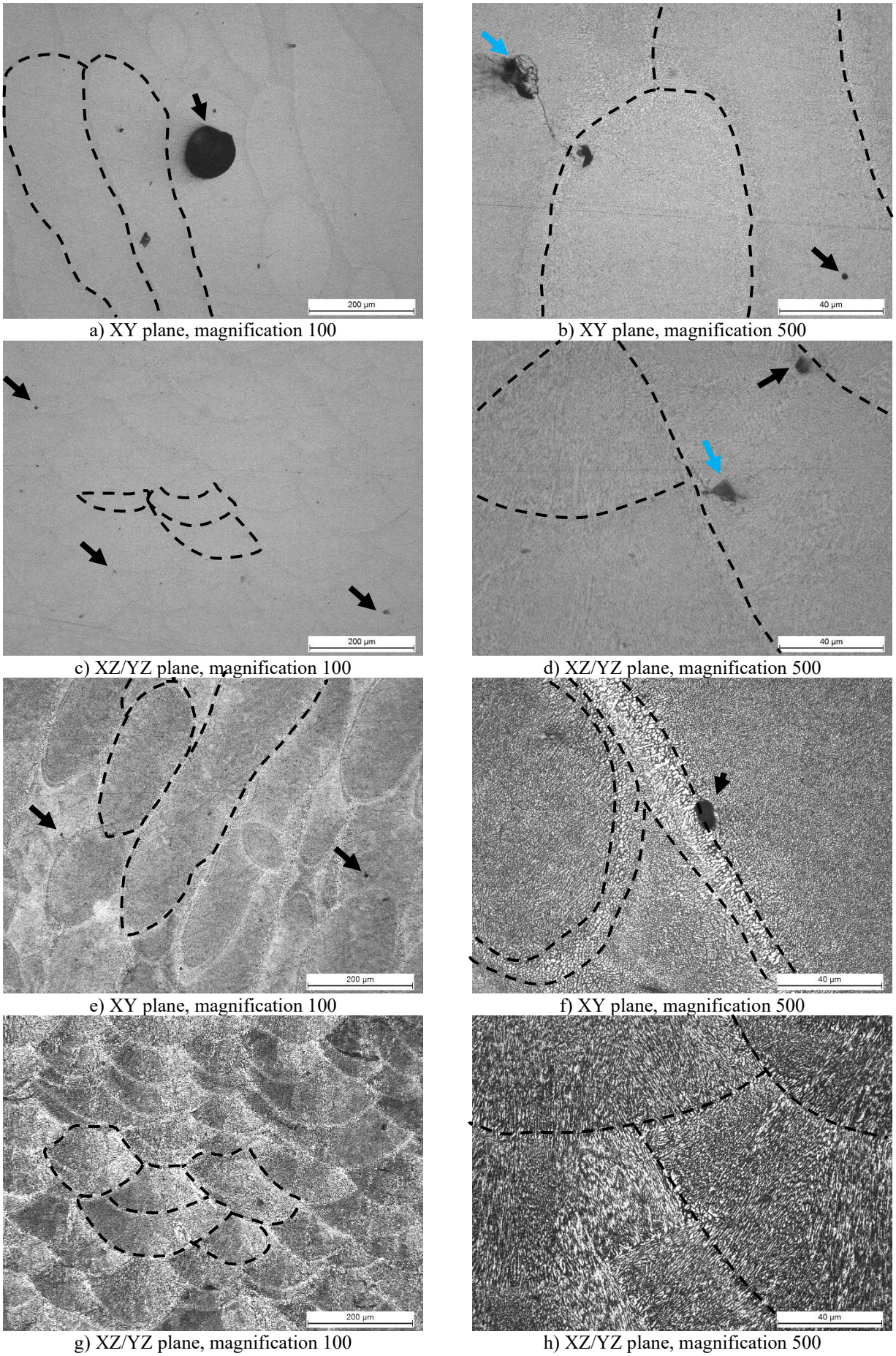


g) XZ/YZ plane, magnification 100



h) XZ/YZ plane, magnification 500

Figure 4. Microstructure of samples produced with Set I parameters; a-d) as polished, e-h) etched.



a) XY plane, magnification 100 b) XY plane, magnification 500

c) XZ/YZ plane, magnification 100 d) XZ/YZ plane, magnification 500

e) XY plane, magnification 100 f) XY plane, magnification 500

g) XZ/YZ plane, magnification 100 h) XZ/YZ plane, magnification 500

Figure 5. Microstructure of samples produced with Set II parameters; a-d) as polished, e-h) etched.

Chemical analysis performed using OES showed that both sets of samples had chemical compositions within the limits specified for EN AC-Al10SiMg alloy. No significant differences were observed between Set I and Set II samples.

Since samples from both sets of parameters were manufactured using powder from the same batch, the absence of compositional deviations confirms that differences in microstructure and defects are attributed to process parameters rather than metal powder variability.

Hardness values measured on XY and XZ/YZ planes showed no significant differences between the two sets of parameters. Set I samples exhibited mean hardness values of 130 HB (XY) and 127 HB (XZ/YZ), while Set II samples showed 130 HB (XY) and 119 HB (XZ/YZ). The results indicate that the difference in LPBF process parameters did not significantly affect bulk hardness. This is expected for AlSi10Mg alloy, where hardness is primarily governed by the fine cellular Al–Si eutectic formed under rapid LPBF cooling conditions. Since both sets of parameters resulted in fine eutectic structure, hardness remained unchanged [10].

5. CONCLUSION

This study investigates the influence of Laser Powder Bed Fusion (LPBF) process parameters on the quality of AlSi10Mg alloy samples. Two sets of samples were produced using different combinations of laser power, scan speed, hatch spacing resulting in two energy densities, 39.3 J/mm^3 for set I, and 50.3 J/mm^3 for set II parameters.

Samples manufactured with lower energy density (Set I) exhibited rougher surfaces, unmelted powder particles, and delamination between layers, indicating insufficient interlayer bonding and lack-of-fusion defects. Samples produced with higher energy density (Set II) showed smoother surfaces and no delamination. Microstructural analysis revealed typical LPBF features in both sets, including fine cellular Al–Si eutectic and coarse dendrite like grains at melt pool boundaries, with pores and lack-of-fusion defects present in all samples but more frequently in Set I samples.

Hardness measurements showed no significant differences between parameter sets or measurement planes. Overall, the results demonstrate that LPBF process parameters strongly affect surface morphology and defect formation, while having negligible influence on bulk hardness. Optimizing energy density is therefore essential for achieving uniform microstructure, adequate layer bonding, and improved part quality in AlSi10Mg components.

Acknowledgement

This work was supported by the Ministry of Science, Technological Development and Innovations (Serbia), Contract No. 451-03-34/2026-03/200325.

Reference

[1] DONG Z., XU M., GUO H., FEI X., LIU Y., GONG B., JU G.. Microstructural evolution and characterization of AlSi10Mg alloy manufactured by selective laser melting, Jouranl of material research and technology,. 17 (2022) 2343-2354.

[2] ABOULKHAIR N. T., SIMONELLI M., PARRY L., ASHCROFT I., CHRISTOPHER T., HAGUE R.. 3D printing of Aluminium alloys: Additive Manufacturing of Aluminium alloys using selective laser melting, Progress in Materials Science, 106 (2019) 100578.

[3] LI W., LI S., LIU J., ZHANG A., ZHOU Y., WEI Q., YAN C., SHI Y.. Effect of heat treatment on AlSi10Mg alloy fabricated by selective laser melting: Microstructure evolution, mechanical properties and fracture mechanism, Materials Science and Engineering: A, 663 (2016) 116-125.

[4] MERTENS A., DELAHAYE J., DEDRY O., VERTRUYEN B., TCHUINDJANG J. T., HABRAKEN A. M.. Microstructure and Properties of SLM AlSi10Mg: Understanding the Influence of the Local Thermal History, Procedia Manufacturing, 47 (2020) 1089-1095.

[5] GHIO E., CERRI E.. Additive Manufacturing of AlSi10Mg and Ti6Al4V Lightweight Alloys via Laser Powder Bed Fusion: A Review of Heat Treatments Effects, Materials, 15(6) (2022) 2047.

[6] TANG M.. Inclusions, Porosity, and Fatigue of AlSi10Mg Parts Produced by Selective Laser Melting, PhD Thesis, Pittsburgh, 2017.

[7] GEBHARDT U., GUSTMANN T., GIEBELER L., HIRSCH F., HUFENBACH H., KÄSTNER M.. Additively manufactured AlSi10Mg lattices – Potential and limits of modelling as-designed structures, Materials & Design, 220 (2022) 110796.

[8] MĚSIČEK J., ČEGAN T., MA Q.-P., HALAMA R., SKOTNICOVÁ K., J. HAJNYŠ, JUŘICA J., KRPEC P., M. PAGÁČ,. Effect of artificial aging on the strength, hardness, and residual stress of SLM AlSi10Mg parts prepared from the recycled powder, Materials Science and Engineering: A, 855 (2022) 143900.

[9] BALLA S. K., MALLAIAH M., NAGAMUTHU S., DAS R. Overview of Laser Powder Bed Fusion and Laser Directed Energy Deposition of Aluminium Alloys: Process, Defects, Microstructure, and Mechanical Properties, Metals and Materials International, 32 (2026) 2584-2623.

[10] GADLEGAONKAR N., BANSOD P. J., LAKSHMIKANTHAN A., BHOLE K.. A Review on Additively Manufactured AISi10Mg Alloy: Mechanical, Tribological, and Microstructure Properties, Journal of Mines, Metals and Fuels, 73(1) (2025) 87-101.